Cavitation Bubbles in Shear Flow

S. Dabiri[1*], W. A. Sirignano[1], and D. D. Joseph[1,2]
[1]Department of Mechanical and Aerospace Engineering
University of California, Irvine, CA 92797, USA
[2]Aerospace Engineering and Mechanics Department
University of Minnesota, Minneapolis, MN 55455, USA

Abstract

Growth and collapse of cavitation bubbles in an orifice flow is simulated in order to understand the effects of bubble deformation and size variation on the flow field. Effects of shear strain, normal strain, and pressure variation are examined. The Navier-Stokes equations are solved by a finite-volume method with a level-set method for interface capturing. Previous experimental studies have shown that cavitation inside liquid injectors improves the atomization process but the physics is not well understood. We observed that the shear in the flow causes the bubbles to deviate from a spherical shape. During collapse of the bubble, two re-entrant jets are formed on sides of the bubble which will collide with each other if the viscosity is small enough. For bubbles with larger surface tension, impingement of re-entrant jets results in breakup of the bubble. A spherical-harmonics decomposition of the velocity field shows the creation of a strong quadrupole field as the bubble collapses. In some cases, the quadrupole component of the velocity exceeds the monopole component.

Introduction

Cavitation in high-pressure liquid injectors strongly influences the flow field [1] and specifically improves the atomization of the emerged liquid jets [2,3]. It has been proposed that the collapse of traveling cavitation bubbles increases the disturbances inside the liquid flow. These disturbances later will trigger the instabilities in the emerged jet, and cause a shorter breakup distance. Different models for cavitation have been proposed that provide good results for vapor fraction and velocity profiles inside nozzle [4]. However, the effects of cavitation on the jet breakup have not been fully understood.

In this study, we have developed a numerical method to simulate growth and collapse of compressible cavitation bubbles in a liquid flowing through an orifice. The full Navier-Stokes equations for multiphase flow are solved. The deformation of bubbles, from a spherical shape, during growth and collapse in the flow depends on the viscous stress, pressure, and the proximity to solid walls. Change in bubble volume and the vorticity generated through change of bubble shape are candidates for the causes of disturbances that enhance jet break-up. The pressure inside the bubble is influenced by both the pressure and the viscous stress in the surrounding liquid. A level-set formulation is used to track the interface and model the surface tension effects. The flow properties including the bubble shape are resolved. The bubble center of mass moves with the average velocity of the displaced fluid. The results will be helpful in understanding the effects of cavitation on the atomization of jets.

Governing Equations and Numerical Method

Navier-Stokes equations are governing the two-phase flow in orifices. The cavitation bubbles grow and collapse in the liquid due to pressure change in the flow. The liquid phase is considered to be incompressible. On the other hand, the bubble is compressible due to the change in the pressure; however, we will assume that the Mach number inside the bubble remains very small. This assumption will exclude the cases of violent bubble collapse from this study where supersonic flow in bubble or even liquid could occur. The bubble is assumed to consist of a non-condensable gas with a uniform density in space. However, the formulation can be easily extended to the case with a mixture of liquid vapor and non-condensable gas in the bubble undergoing isentropic or polytropic expansion and/or collapse.

We assume that the density variation in space inside the bubble is negligible. Assuming that bubble goes through a polytropic process, one can find the density as a function of pressure from the equation of state. Thus, the Lagrangian derivative of density in the continuity equation for the gaseous phase can be written as

---

* Corresponding author

$$\nabla \cdot u = -\frac{1}{\overline{\rho}} \frac{d\overline{\rho}}{d\overline{P}} \frac{d\overline{P}}{dt} \qquad (1)$$

$\overline{P}$ and $\overline{\rho}$ are the average pressure and density inside the bubble. The average pressure in the bubble is used instead of local pressure in order to suppress the acoustic wave propagation inside the bubble. The numerical solution of the unsteady Navier-Stokes equations is performed using the finite-volume method on a staggered grid. The convective term is discretized using the Quadratic Upwind Interpolation for Convective Kinematics (QUICK) (by Hayase [5]). The Semi-Implicit Method for Pressure-Linked Equation (SIMPLE), developed by Patankar [6] is used to solve the pressure-velocity coupling. The time integration is accomplished using the second-order Crank-Nicolson scheme. A level-set method is used to capture the interface and model the surface tension effects.

Results and Discussion

Cavitating flows in orifices have a wide range of time and length scales due to presence of micron size cavitation bubbles in the orifice. In order to overcome the difficulties of numerical simulation of such a system, a one-way interaction between the bubbles and the orifice flow is considered first. In this approach, the orifice flow is solved first without bubbles and then the solution for pressure and shear in the orifice are used to create a similar environment for an individual cavitation bubble.

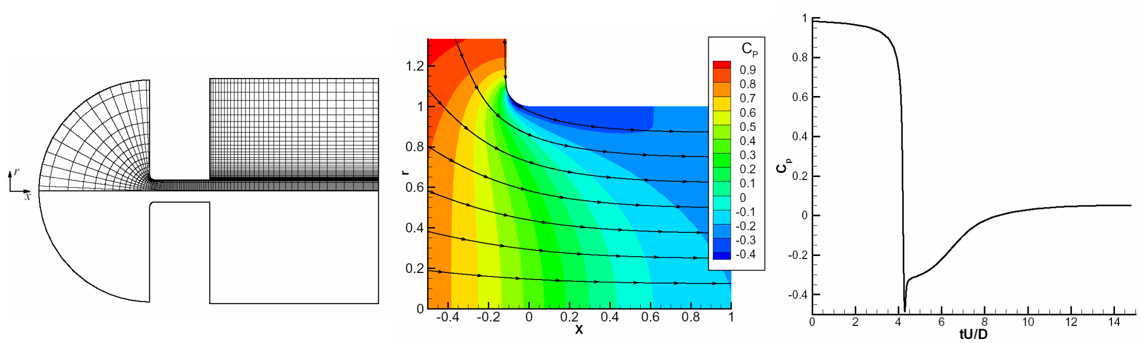

Figure 1. Flow through an orifice at Re = 8000: *left*, geometry of the axisymmetric orifice and the boundary fitted grid; *center*, pressure coefficient contours and streamlines; *right*, history of the pressure coefficient felt by a fluid element as it travels through the orifice. The streamline that passes near the orifice corner is used to find pressure history.

Figure 1 shows the orifice geometry and the computational domain in which the axisymmetric and laminar orifice flow is solved. We are interested in the flow near the upstream corner of the orifice, where the flow is still laminar. Liquid at high pressure on left flows through the orifice to the low-pressure ambience on the right. No slip boundary conditions are applied on the orifice wall and zero Lagrangian derivative is applied on the downstream boundary. Mass flux is specified on the upstream boundary. More details can be found in Dabiri *et al.*[7] The solution of the orifice flow is shown in Figure 1. The calculation is performed for flow with a Reynolds number of Re = 8000 based on the orifice diameter. A region of low pressure is present behind the inlet of the nozzle. This is where the cavitation inception will most likely occur. High levels of vorticity are also present at this point due to the boundary layer that separates from the nozzle wall downstream of the corner.

Now, we assume that any bubble in the flow will travel with the local velocity of the flow field. Therefore, by tracking a material point in the orifice one can find the pressure and shear rate that is felt by the particle. The particle path that has been chosen is the one that is closed to the orifice corner as shown in Figure 1. This figure also shows the pressure history as an element of mass passes through the orifice. The pressure drop occurs near the nozzle inlet and then the pressure recovers to the downstream pressure value. This pressure profile then is applied as a time varying boundary condition for a bubble that grows and collapses in a shear flow and/or extensional flow. The computational domain consists of a cubic Cartesian grid with a simple shear flow, $u = k_s y$, and/or a two dimensional extensional flow, $u = k_n x$; $v = -k_n y$. The amount of shear rate or normal strain rate also comes from the orifice calculations. However, a constant strain rate is applied that does not vary with time and its value is the average value of the strain rate on the path of the bubble through the orifice. The bubble is initially spherical and is placed in the center of the computational domain. The frame of reference is attached to the center of mass of the bubble; so, the center of mass of the bubble does not move during the simulation. Moreover, considering the symmetry (over the x-y plane) and antisymmetry in the problem, one needs to solve only a quarter of the domain, by applying correct boundary conditions. The antisymmetry condition is represented as

$$u(x,y,z) = -u(-x,-y,z); \quad v(x,y,z) = -v(-x,-y,z); \quad w(x,y,z) = w(-x,-y,z) \tag{2}$$

Based on the governing equations, seven dimensionless parameters can be defined as follow:

$$\mathrm{Re} = \frac{\rho_l k R_o^2}{\mu_l}, \quad We = \frac{\rho_l k^2 R_o^3}{\sigma}, \quad \alpha = kR_o\sqrt{\frac{\rho_l}{\Delta P}}, \quad \beta = \frac{R_o}{D}, \quad K = \frac{\Delta P}{P_d} \tag{3}$$

Two other dimensionless parameters are the liquid-to-gas density ratio and viscosity ratio, both having a value of 100 initially. Reynolds and Weber numbers are defined based on the shear rate, k, and initial radius of the bubble, R_o. α defines the ratio of shear stress to the pressure drop across orifice, β is the ratio of the bubble radius to the orifice diameter, D, and K is the ratio of the pressure drop across the orifice to the downstream pressure, P_d. Note that different and much larger Reynolds number and Weber number can be defined based on the orifice exit velocity corresponding to the pressure drop. The pressure drop across the orifice is of the same order of magnitude as the pressure difference across the liquid layer surrounding the bubble. Consequently, the normal velocity at the bubble surface will be of the same order as the orifice exit velocity. Table 1 provides a list of parameters used in this study.

Table 1. List of parameters for different cases.

Case	Re	We	α	β	K	Flow type
Case 1	1.0	0.1	0.015625	0.003125	2.0142	Shear
Case 2	0.5	0.1	0.015625	0.003125	2.0142	Shear
Case 3	1.242	0.02984	0.0352	0.004405	2.5617	Shear

Figures 2-4 show snapshots of the cavitation bubble from the instant it reaches its maximum volume until it collapses and rebounds. Cross section of the bubble, velocity distribution and pressure and vorticity contours are shown in each figure. Lengths are normalized by the initial radius of the bubble and time is normalized by the inverse of the shear rate. The first image in Figure 2 shows the bubble at its maximum volume. This maximum volume occurs slightly after the pressure reaches its minimum and starts to recover. This is due to the inertia of the liquid. At the maximum volume, the bubble has an ellipsoidal shape which is a result of the shear flow. As the bubble collapses, two regions of high pressure are formed on upper right and lower left sides of the bubble. These high pressure regions later lead to creation of two re-entrant jets on both sides of the bubble. The formation of high pressure region and re-entrant jets are similar to what has been observed during collapse of cavitation bubbles near rigid walls. However, in that case only one re-entrant jet is formed that collides with the other side of the bubble. On the other hand, the two re-entrant jets, here, impinge on each other and create a liquid sheet. The impingement occurs at t = 1.315, slightly after the bubble has reached its minimum volume at t = 1.302. Then, the bubble rebounds and the impinging jets create a liquid sheet inside the bubble. In this case, the bubble remains integrated and does not break up into smaller bubbles.

The effects of viscosity have been studied by considering a lower Reynolds number in Case 2. The results are shown in Figure 3. The bubble at its maximum volume is very similar in shape to Case 1. Also, during the collapse phase, the high pressure regions near the sides of the bubble are observed. However, the re- entrant jets are not as strong as before and they start to form later in time compared to Case 1. In this case, the re-entrant jets do not have enough momentum to overcome the viscous forces and they don't penetrate the bubble much and specifically they do not impinge on each other. Similar behavior is observed during collapse of cavitation bubbles near rigid walls by Popinet and Zalesky [8]. They found that the larger viscosity of the liquid prevents the re-entrant jet to collide on the other side of the bubble.

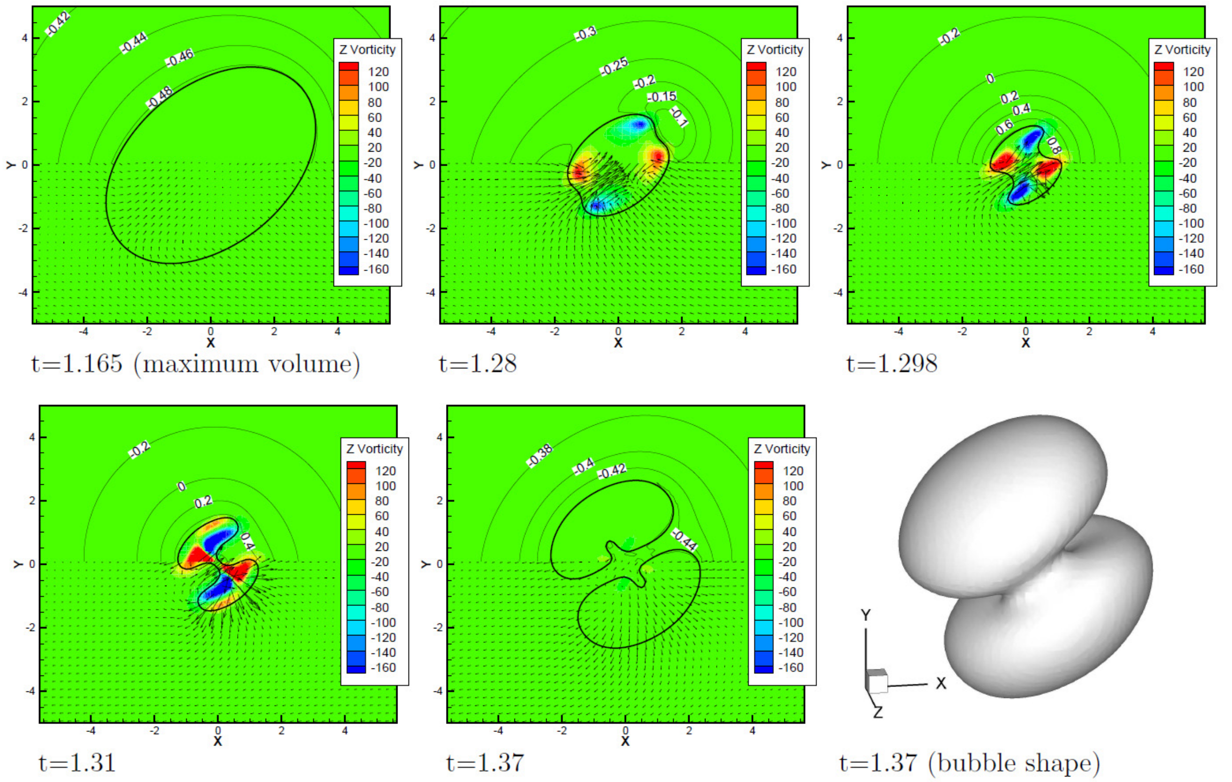

Figure 2: Growth, collapse and rebound of cavitation bubble in shear flow for Case 1, $Re = 1.0, We = 0.1$. Bubble interface, velocity vectors and pressure coefficient contours are shown in the plane of symmetry of the bubble.

Another case that has been studied is shown in Figure 4. This case represents a higher surface tension coefficient and lower Weber number. Similarly, as the bubble collapses the high pressure regions and re-entrant jets form on sides of the bubble. However, in this case, the jets are wider and have a size comparable to the size of the bubble itself. When the jets collide with each other, the bubble breaks up into two parts, while expanding in a direction normal to the shear flow. This high surface tension results in a capillary necking action which together with the re-entrant jets leads to bubble fracture. The independency of the results on the computational grid size has been checked by repeating the calculation for Case 3 on a finer grid. The finer grid has fifty percent more nodes in each of *x, y* and *z* directions. The maximum volume of the bubble calculated from the finer grid is only 5% different than the regular grid that has been used.

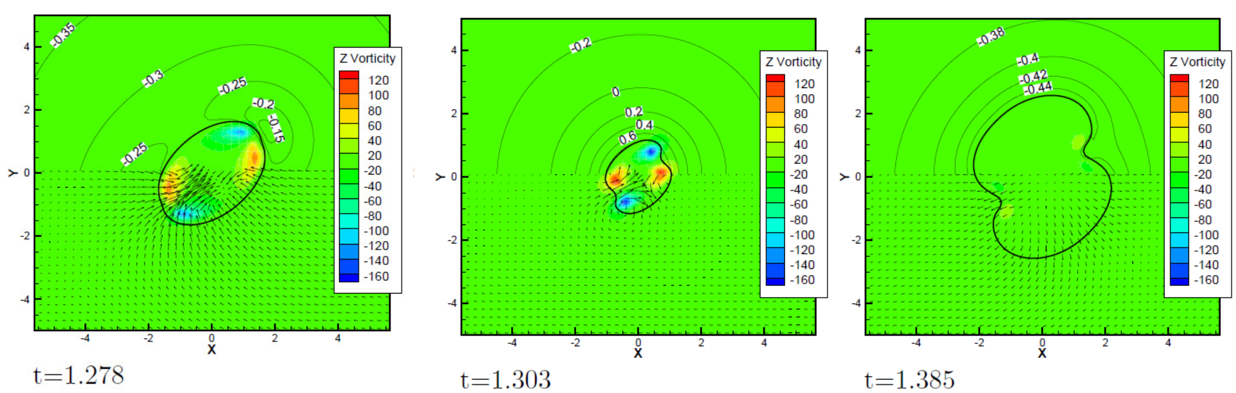

Figure 3: Growth, collapse and rebound of cavitation bubble in shear flow for Case 2, $Re = 0.5, We = 0.1$. Bubble interface, velocity vectors and pressure coefficient contours are shown in the plane of symmetry of the bubble.

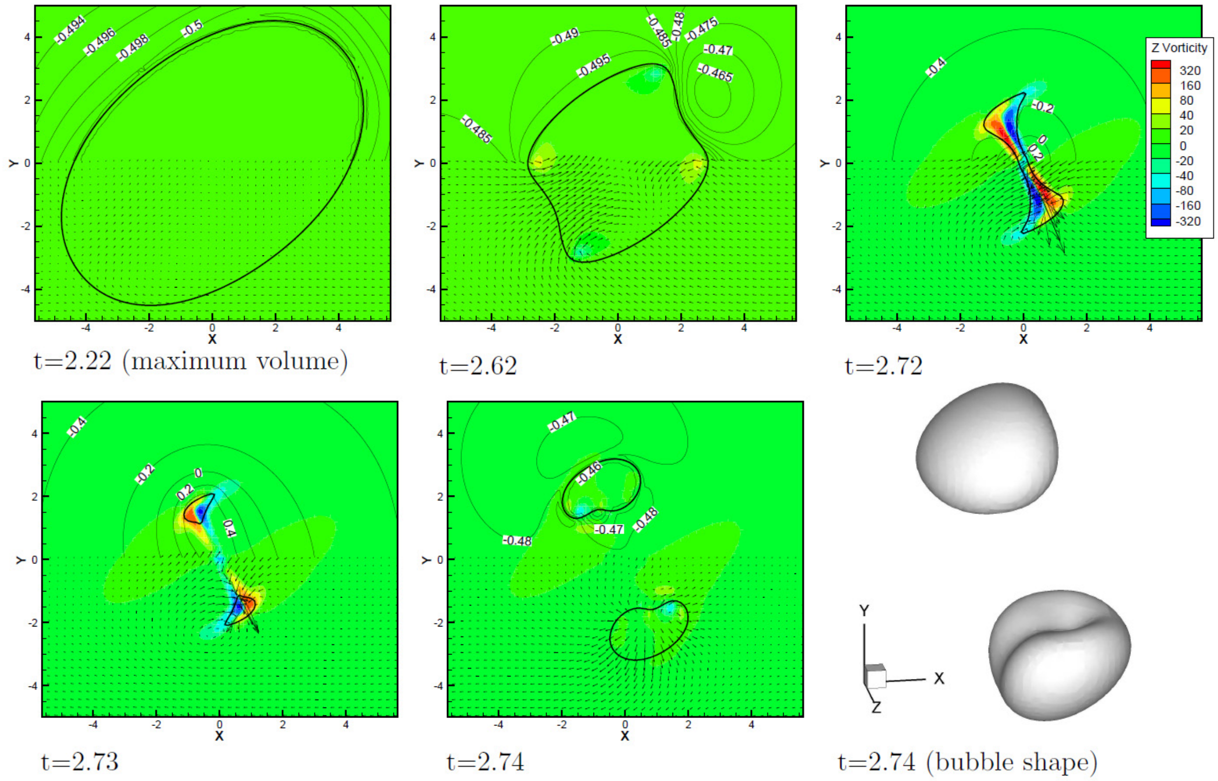

Figure 4: Growth, collapse and rebound of cavitation bubble in shear flow for Case 3, $Re = 1.242, We = 0.02984$. Bubble interface, velocity vectors and pressure coefficient contours are shown in the plane of symmetry of the bubble.

Observing the velocity field near the bubbles during growth and collapse, we found that, in addition to monopole source or sink velocity field and a base shear flow, there exists a quadrupole velocity field that is produced by antisymmetrical growth and collapse of the bubble. The velocity field can be expanded in terms of spherical harmonics to extract more information about the strength of monopole and quadrupole terms. Results of this analysis are shown in Figure 5. The solid lines represent the component of velocity field corresponding to a monopole and dashed lines represent the component of velocity field for three quadrupoles. As can be seen, the quadrupoles can create a velocity as strong as monopoles. The largest component of quadrupole always remains in the x-y plane which is the plane of shear flow. It appears that the largest quadrupole component correlates well with the monopole component. One might note that the dipole velocity field generated by bubble deformation is zero due to the antisymmetry in the problem. Vorticity generation by the bubbles has also been investigated by integrating over the plane of symmetry of the bubble. Results are presented in Figure 5. Integration has been divided to positive and negative parts, which are defined as

$$\Gamma^+ = \int_\Omega \max(\omega + k, 0)\,dA, \qquad \Gamma^- = \int_\Omega \left|\min(\omega + k, 0)\right| dA \qquad (4)$$

where $-k$ is the vorticity of the base flow that has been subtracted. As can be seen in the figures, vorticity integrals peak at the same time as quadrupoles peaks.

The bubble in extensional flow is also under investigation. In this case, the bubble has a triple symmetry. The bubble at its maximum volume has a prolate shape with longest axis along the *x*-axis. When the bubble collapses, it changes to an oblate shape with shortest axis in *x* direction. In this case, no re-entrant jet is observed and the bubble does not break up.

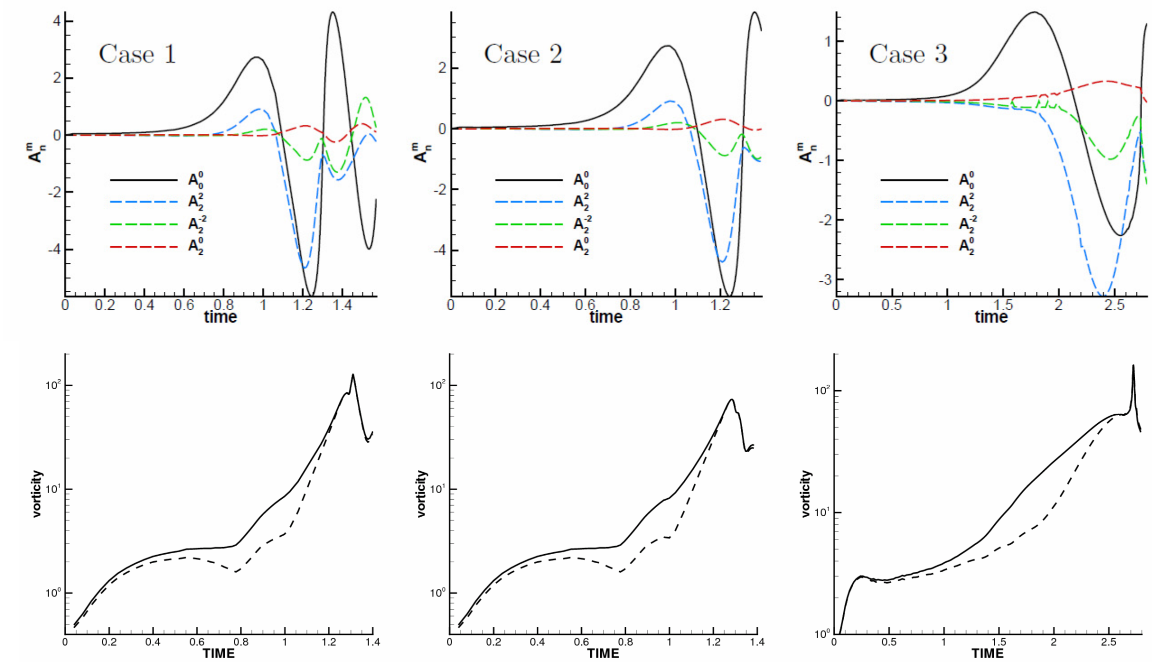

Figure 5: *Top*: Amplitude of spherical harmonics in the velocity field around the bubble at r=4, including monopole (solid line) and quadrupoles (dashed lines); *bottom*: positive vorticity integral (solid lines) and negative vorticity integral (dashed lines) over the plane of symmetry.

Conclusions

Navier-Stokes equations for two phase flow are solved to model growth and collapse of cavitation bubbles in the shear flow. A variable pressure boundary condition is imposed which is extracted from solution of viscous flow through an orifice. Re-entrant jets are formed on the bubbles as they collapse. Impingement of these jets could result in break up of the cavitation bubble into two bubbles in some cases. The re-entrant jets achieve high velocities during the collapse phase and could increase disturbances in the flow. It is known that in a bubbly flow, monopoles are created by pressure changes and dipoles are created by acceleration of the flow; we have found that quadrupoles are also created when there is a strain, shear or extensional, in the base flow. The size of the quadrupoles correlates with the monopole component and they can create velocity fields as strong as the velocity field created by monopoles.

Acknowledgement

This research has been supported by the US Army Research Office through grant No. W911NF-06-1-0225, with Dr. Kevin McNesby and Dr. Ralph Anthenien having served sequentially as program managers. D. D. Joseph was also supported by NSF grant No. CBET-0302837.

References

1. He, L., Ruiz, F., *Atomization and Sprays* 5:569-584 (1995).
2. Tamaki, N., Shimizu, M., Hiroyasu, H., *Atomization and Sprays*, 11:125 (2001).
3. Hiroyasu, H., *mization and Sprays*, 10:511-527 (2000).
4. Giannadakis, E., Papoulias, D., Gavaises, M., *SAE Technical Paper*, No. 2007-01-0245 (2007).
5. Hayase, T., Humphrey, J. A. C., Greif, R., *J. Comput. Physics*, 98:108-118 (1992).
6. Patankar, S. V., *Numerical heat transfer and fluid flow*, Hemisphere, 1980.
7. Dabiri, S., Sirignano, W. A., and Joseph, D. D., *Physics of Fluids*, 19:7, 072112 (2007).
8. Popinet, S. and Zaleski, S., *Journal of Fluid Mechanics*, 464:137-163 (2002).